Received: 11 April 2022 | Accepted: 17 April 2022

DOI: 10.1111/ahe.12806

ORIGINAL ARTICLE

ANATOMIA HISTOLOGIA EMBRYOLOGIA JOURNAL OF VETERINARY MEDICINE WILEY

Computed tomography venography description of the normal anatomy of the canine hindlimb venous system

Klara Theresia Besuden | Andrea Meyer-Lindenberg | Andreas Brühschwein

Clinic for Small Animal Surgery and Reproduction, Ludwig-Maximilians-University, Munich, Germany

Correspondence
Klara Theresia Besuden, Clinic for Small Animal Surgery and Reproduction, Ludwig-Maximilians-University, Munich, Germany.
Email: klara.besuden@lmu.de

Abstract

This study was performed to provide a description of the normal anatomy of the canine hindlimb veins using helical CT images. The studies of 30 dogs that underwent CT venography with a 64-slice helical CT scanner were retrospectively reviewed. The dogs were positioned in a head-first prone or head-first supine body position. A topogram CT scan was performed from the pelvic limbs cranial to the iliac wings to the tips of the paws. Bolus-tracking software was used for the dual-phase angiogram, and contrast medium was administered in a cephalic vein. The venous phase was scanned after a delay time of a few seconds after the arterial phase in a caudocranial direction. Three-dimensional images were generated using maximum intensity projections and volume rendering technique. Representative images of three of the 30 dogs were selected and anatomic structures labelled.

KEYWORDS
anatomy, canine, computed, hind limb, tomography, venography

1 | INTRODUCTION

Very soon after the introduction of computed tomography (CT) in human medicine in 1980, Zerhouni et al. (1980) were able to detect venous thrombi in the inferior vena cava and the iliac veins in computed tomography based on the anatomy of the vein. As one of the first Stehling et al. (1994) described the injection of intravenous contrast medium in each foot and assessment of the veins with helical CT venography. Current studies show that the use of contrast medium in computed tomography angiography (CTA) is the investigational tool of choice for imaging and assessing lower limb veins and especially in the pelvis (Lee et al., 2008; Liu et al., 2018; Wright et al., 2017). This is, in human medicine, shown to be particularly important, where venous thromboembolism is a major health problem (Aquila, 2001; Shiver et al., 2010). The most frequent localization of deep vein thrombosis (DVT) in humans is at lower limbs (Erdmann et al., 2015).

In human medicine, when searching for DTV, especially when DTV is suspected to be associated with pulmonary embolism, a review by Katz et al. (2002) revealed that CT venography is an accurate imaging option when searching for venous thrombi and showed the broad spectrum of venous and extravenous findings that can be detected in the CT venographic phase. It is often incorporated in CTA protocols in human medicine (Kanne and Lalani, 2004).

Despite the lower incidence of deep vein thrombosis in dogs, it can also be found in canine hindlimbs, especially in dogs with parvoviral enteritis, shown by a study of Otto et al. (2000). Most important when using CTA to diagnose vascular anomalies and abnormalities is familiarity with the normal anatomy of the vasculature on cross-sectional imaging. Therefore, the aim of the present study was to provide a description of the normal anatomy of the canine hindlimb veins using helical CT images.

2 | MATERIAL AND METHODS

2.1 | Dogs

30 pelvic limbs of dogs of different breeds, sizes (3.7 to 65 kg) and ages (3 to 164 months) from the patient population of the Clinic for Small Animal Surgery and Reproduction of the Ludwig-Maximilians-University Munich were examined by CTA. The images were retrospectively reviewed. The selected patient population consisted of dogs that underwent CT examination of the caudal body region with multiple contrast phases for orthopaedic, surgical, genitourinary or purely diagnostic purposes. Indications for CTA included suspected ectopic ureter, or clarification of hindlimb lameness. Inclusion criteria were a gapless scan of the entire hindlimb of the dog as well as good detectability of the veins with sufficient accumulation of contrast media. Exclusion criteria were a venous catheter in a hindlimb, high-grade flexion or high-grade asymmetric body position and diseases that would have been highly likely to affect the course or visualizability of the hindlimb veins.

2.2 | Computed tomography angiography

The dogs were anaesthetized through the administration of various pre-anaesthetics via intravenous catheter in a cephalic vein. Each dog received propofol in a bolus of 2–3 mg/kg and was intubated. Anaesthesia was maintained with 2% isoflurane and an oxygen gas mixture. Monitoring of the patients included heart rate as well as carbon dioxide capnography and pulse oximetry. 26 dogs were positioned in head-first supine position and 4 dogs in head-first prone position on the CT Table. 27 dogs were positioned with symmetrical extended hindlimbs, and three dogs needed to be positioned in frog position.

The examination was performed with the 64-slice helical CT scanner SOMATOM Definition AS, CT070/13/S, from Siemens AG (Siemens Healthcare GmbH, Erlangen, Germany) with parameters of 120 mAs, 120 kV, 512 x 512 image size matrix, 0.6 mm slice thickness, rotation time 0.5 s and FOV as small as possible, but as large as necessary and a kernel setting of B26f for all acquired data.

For intravenous administration of the non-ionic, monomeric, triiodinated, water-soluble contrast agent iohexol (Accupaque 300,

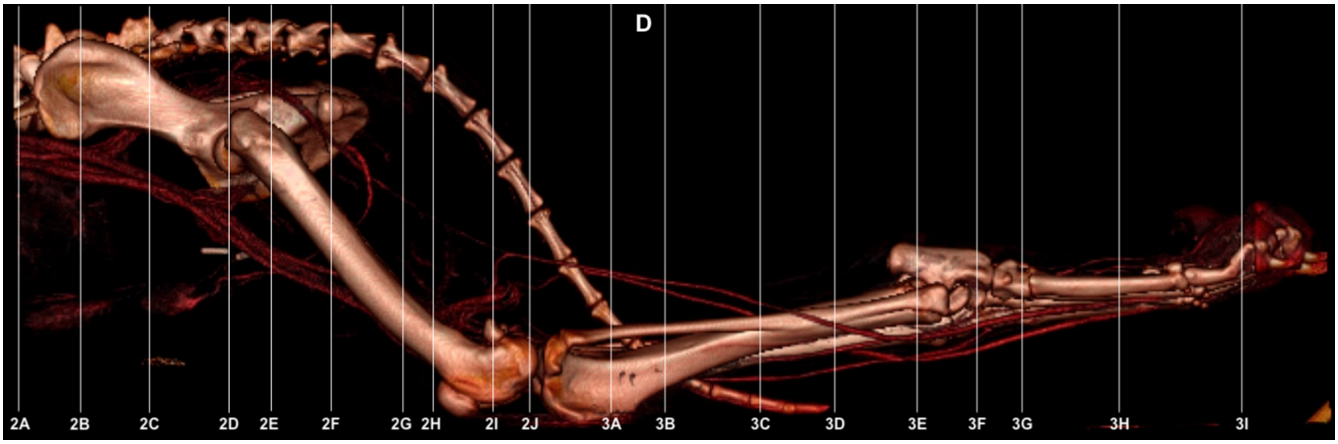

FIGURE 1 Lateral VRT 3D image of the canine hindlimb to illustrate cross section 2 A to 3 I in the venous phase of CT angiography

FIGURE 2 Transverse CT images of the normal canine caudal abdomen and thigh of a dog in the venous phase of angiography at the different levels, shown in Figure 1. Window (WW = 350; WL = 40). The dogs were positioned in sternal recumbency (D) dorsal; (V) ventral; (L) left; (R) right. (a) (1) Lumbar vertebra V; (2) caudal vena cava; (3) abdominal aorta; (4) psoas major muscle; (5) iliocostal muscle; (6) lumbar multifidus muscle; (7) lumbar longissimus muscle. (b) (1) Lumbar vertebra IV; (2) wing of ilium; (3) right common iliac vein; (4) left common iliac vein; (5) urinary bladder; (6) psoas minor muscle; (7) sartorius muscle; (8) tensor fasciae latae muscle; (9) medial gluteus muscle; (10) iliocostal muscle; (11) lumbar multifidus muscle; (12) adipose panicle; (13) left external iliac artery; (14) abdominal aorta. (c) (1) Right external iliac vein; (2) right external iliac artery; (3) right internal iliac vein; (4) right internal iliac artery; (5) right cranial gluteal vein; (6) third sacral vertebra; (7) iliac bone; (8) right prostatic vein. (d) (1) Right femoral head; (2) right acetabulum; (3) right external pudenda vein; (4) right deep femoral vein; (5) right femoral vein; (6) right lateral circumflex femoral vein; (7) right lateral circumflex femoral artery; (8) right femoral artery; (9) right ascending branch of lateral circumflex femoral vein; (10) right caudal gluteal vein; (11) right caudal gluteal artery; (12) right medial gluteal muscle; (13) right quadriceps femoris muscle; (14) right iliopsoas muscle; (15) right pectineus muscle. (e) (1) Right obturator vein branch of medial circumflex femoral vein; (2) right deep femoral vein; (3) right femoral vein; (4) right caudal superficial epigastric vein; (5) caudodistally directed muscle branches of right deep femoral vein branching out in adductor muscles; (6) right caudal gluteal vein; (7) right caudal gluteal artery; (8) pubic bone; (9) right caudal lateral superficial vein. (f) (1) Iliac bone wing; (2) femoral marrow; (3) femoral artery; (4) femoral vein; (5) right testicular vein; (6); (7) right caudal gluteal vein; (8) right internal pudendal vein; (9) right adductor magnus and brevis muscle; (10) right quadriceps femoris muscle; (11) right caudal lateral superficial vein. (g) (1) Right femoral marrow; (2) right femoral vein; (3) right femoral artery; (4) right proximal caudal femoral vein; (5) right caudal lateral superficial vein; (6) right medial saphenous vein; (7) testicle. (h) (1) Right medial caudal femoral vein; (2) right femoral vein. (i) (1) Right distal caudal femoral vein; (2) right popliteal vein; (3) right medial saphenous vein; (4) right medial fabella; (5) right distal femur epiphysis. (j) (1) Lateral condyle of left femur; (2) genicular vein; (3) left popliteal vein; (4) left caudal femoris distalis vein; (5) left caudal femoris distalis artery

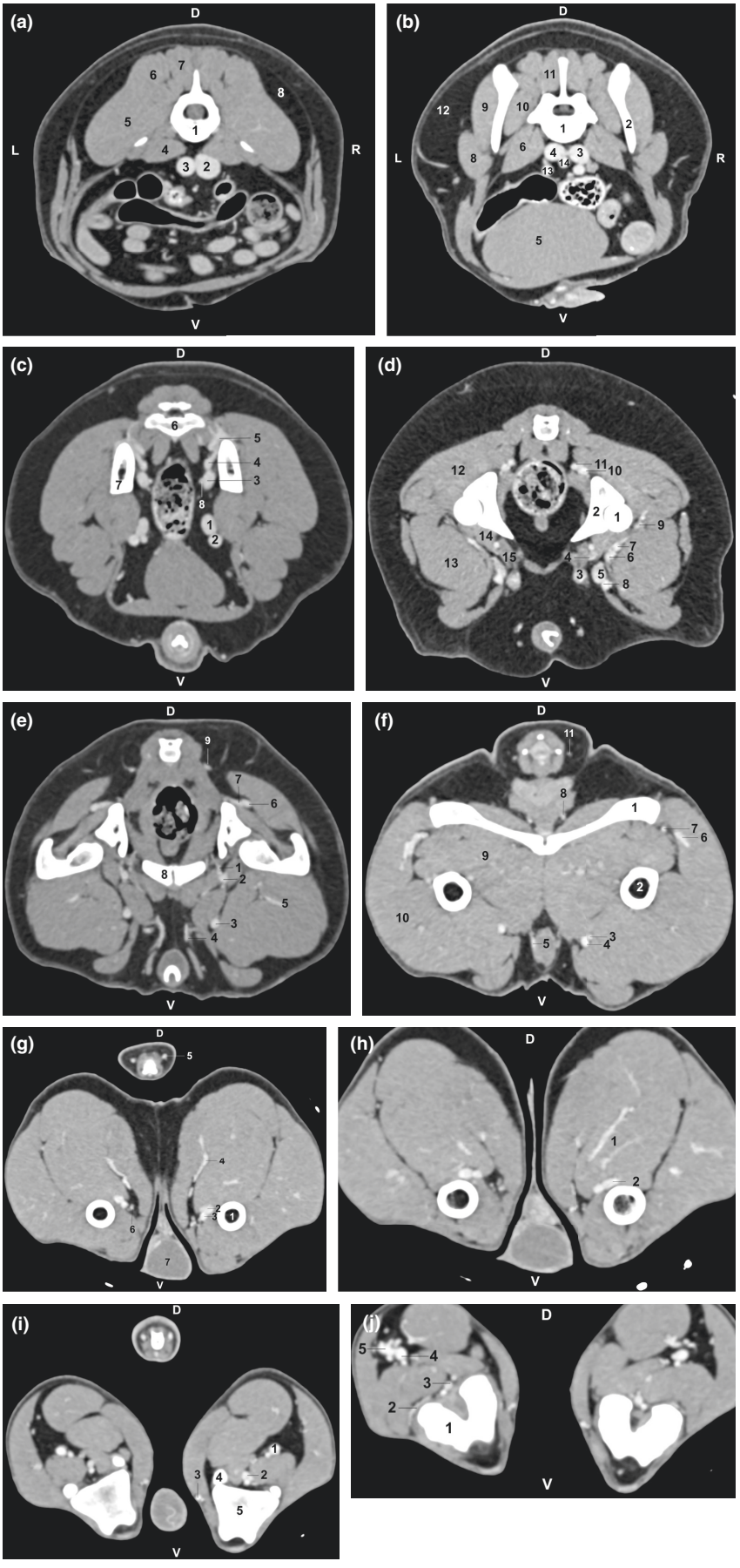

GE Healthcare Buchler GmbH & Co. KG, Braunschweig, Germany) in the cephalic veins, the fully automated contrast agent applicator MEDRAD Stellant (Bayer Vital GmbH, Bayer Healthcare Radiology, Leverkusen, Germany) was used. Iohexol was used at a dosage of 2 ml/kg body weight, what contains an iohexol concentration of 647 mg/ml, which corresponds to a bound iodine concentration of 300 mg iodine/ml. Depending on the size of the vein catheter, flow rates of 0.5 to 3.5 ml/s were used for injection. Before and after the iohexol application, the dogs received NaCl 0.9% boluses of 5 to 20 ml, depending on their body weight. The region of interest was set using a topogram and included the region of the pelvic limbs cranial to the iliac wings to the tips of the paws. Bolus-tracking software was used. The premonitoring and monitoring phases of the programme used a cross-sectional image from the native scan to determine a reference layer in which contrast agent accumulation in the patient's descending aorta could be detected and served as a starting point for bolus tracking. After reaching the threshold of 100 HU in the abdominal aorta, the arterial scan of the study region was started automatically and in cranio-caudal direction down to the paw tips proximodorsally. The venous phase was scanned immediately after the arterial phase in caudocranial and distoproximal direction, respectively. Depending on the size of the dog, every scan took between 5 and 30 s.

Images from all dogs were studied, and vessels were identified using textbooks on canine anatomy (Budras et al., 2007; Habermehl et al., 2005).

The dogs DICOM studies were retrieved and reconstructed at syngo CT Workplace (Siemens Healthcare GmbH, Erlangen, Germany). Image viewing and analysis as well as maximum intensity projections and 3D volume rendering images were performed and generated using medical imaging software Horos™ (version 3.3.6, http://www.horosproject.org/, open source, © 2022 Horos Project).

The three dogs whose veins could be best identified and followed in their course were selected for depiction in the figures.

3 | RESULTS

The results of this study comprise the CT images presented in Figures 1–6. The same structures were identified in all dogs, and the images of all dogs were similar. The images are presented in a cranial to caudal progression from the level of the pelvic inlet to the paw claw tips. Identifiable anatomical structures and veins are labelled on the CT images. Several veins, such as the common iliac vein, the internal iliac vein, the external iliac vein, the deep femoral vein, the femoral vein, the caudal femoris distalis vein, the lateral saphenous vein and the plantar metatarsal veins, were easily identified during the venous phase. The external iliac vein was identified in all 30 dogs as a lateral division branch of the common iliac vein located distally to the sacrum (Figure 2c/1). The branching into the deep femoral vein (Figure 2d/4) was located proximal to the femoral canal, and the vein could be followed into the adductor muscles in 12 dogs (40%). The external iliac vein continued as the femoral vein (Figure 2d/5), which could be traced running distally in the femoral canal and caudally halfway along the femur through the adductor muscles to the popliteal fossa (Figure 2e/3, f/4, g/2 and h/2) in all 30 dogs. The cranial gluteal vein branched from the internal iliac vein at the level of third sacral vertebra and could be traced in its course through the greater sciatic notch into the gluteus musculature (Figure 2c/5) in 7 dogs (23.3%). The prostatic vein originated from the internal iliac vein at the level of the cranial aperture of pelvis (Figure 2c/8), visible in 5 of the 14 male dogs (35.7%). The external pudenda vein (Figure 2d/3) branched from the pudendoepigastrical vein and could be followed through the femoral canal in 9 dogs (30%). The lateral circumflex femoral vein arised proximally in the femur canal from the femoral vein and could be detected in 17 dogs (56.7%). The ascending and descending branches of the lateral circumflex femoral vein (Figure 2d/6) were identified and traced to the gluteal and adductor muscles in 11 dogs (36.7%). The medial circumflex femoral

FIGURE 3 Transverse CT images of the normal canine lower leg and paw of a dog in the venous phase of angiography at the different levels, shown in Figure 1. Window (WW = 350; WL = 40). The dogs were positioned in sternal recumbency. (D) Dorsal; (V) ventral; (L) right; (R) right. (a) (1) Compact bone of right tibia head; (2) neck of right fibula; (3) right popliteal lymph node; (4) right lateral saphenous vein; (5) right medial saphenous artery; (6) right medial saphenous vein. (b) (1) Compact bone of right tibia body; (2) body of right fibula; (3) right lateral saphenous vein; (4) caudal branch of medial saphenous vein; (5) cranial branch of medial saphenous vein; (6) left cranial tibial vein; (7) left cranial tibial artery. (c) (1) Right distal tibia epiphysis; (2) right fibula; (3) right lateral saphenous vein; (4) caudal branch of right medial saphenous vein; (5) left cranial tibial vein; (6) cranial branch of left medial saphenous vein. (d) (1) Right distal tibia epiphysis; (2) right fibula; (3) cranial branch of right lateral saphenous vein; (4) caudal branch of right lateral saphenous vein; (5) calcaneal branch of right lateral saphenous vein; (6) caudal branch of right medial saphenous vein; (7) cranial branch of right medial saphenous vein; (8) right cranial tibial artery; (9) common calcaneal tendon; (10) extensor digitorum longus muscle; (11) cranial tibial muscle. (e) (1) Right distal tibia; (2) right distal fibula; (3) right calcaneal tuber; (4) anastomosis and in parts common course of the right cranial branches of the medial and lateral saphenous veins; (5) caudal branch of the right lateral saphenous vein; (6) caudal branch of the right medial saphenous vein; (7) right cranial tibial vein; (8) right cranial tibial artery; (9) anastomosis and immediately separation of the cranial branches of the left medial and lateral saphenous veins; (10) left medial tarsal vein. (f) (1) Left calcaneus; (2) left talus; (3) caudal branch of right medial saphenous vein; (4) superficial plantar branch of right medial tarsal vein; (5) right medial tarsal vein; (6) right dorsal pedal vein merging into cranial branch of medial saphenous vein; (7) cranial branch of lateral saphenous vein; (8) right lateral tarsal vein; (9) caudal branch of lateral saphenous vein. (g) (1) Left calcaneus; (2) left talus head; (3) right medial and lateral plantar vein; (4) right medial tarsal vein; (5) cranial branch of medial saphenous vein; (6) cranial branch of lateral saphenous vein; (7) deep plantar arch. (h) (1) Left metacarpal bone II; (2) right superficial plantar branch of medial tarsal vein; (3) right plantar metatarsal vein II; (4) right common digital dorsal veins; (5) right superficial branch of caudal branch of lateral saphenous vein. (i) (1) Right proper plantar digital veins; (2) left proper dorsal digital veins

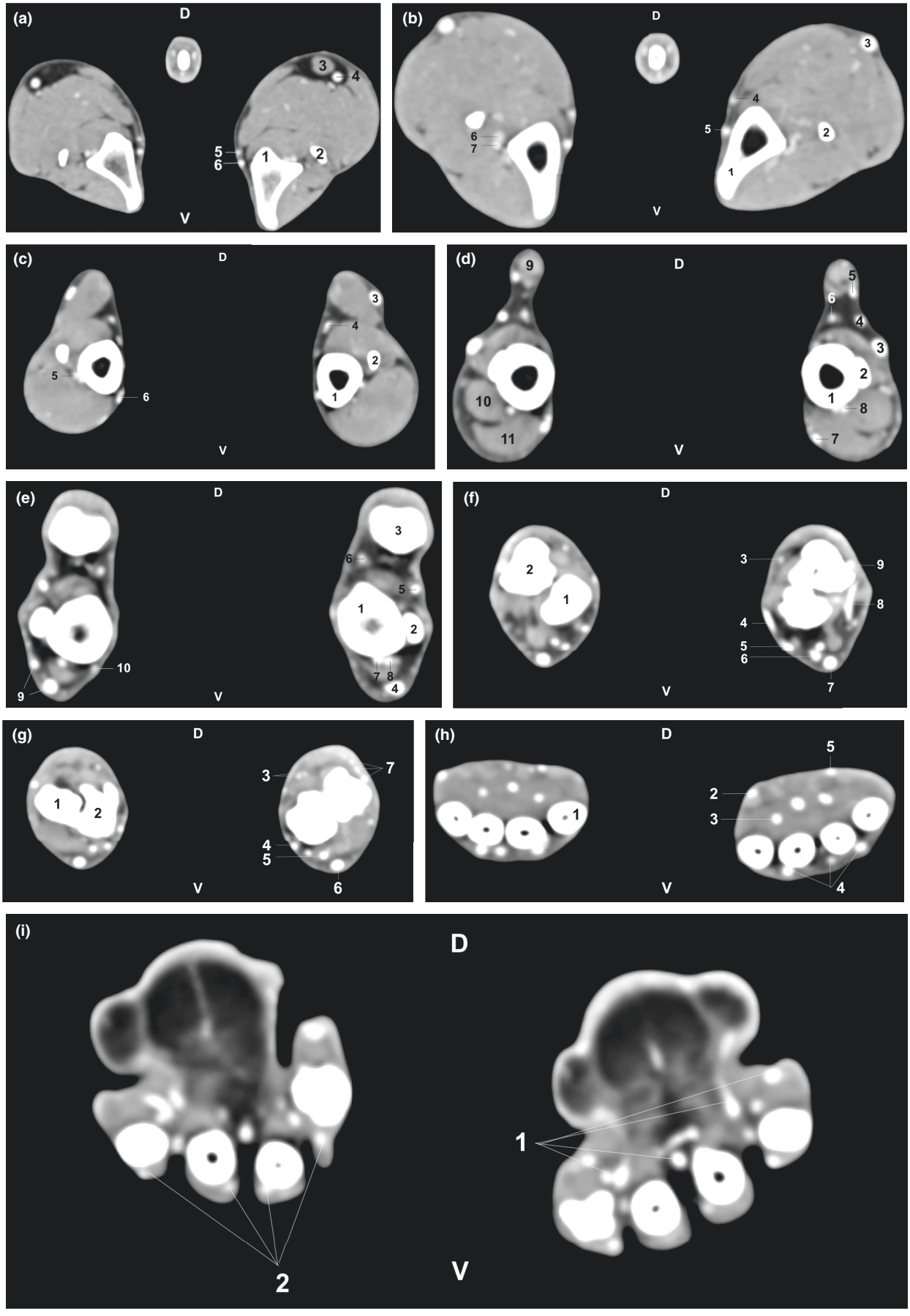

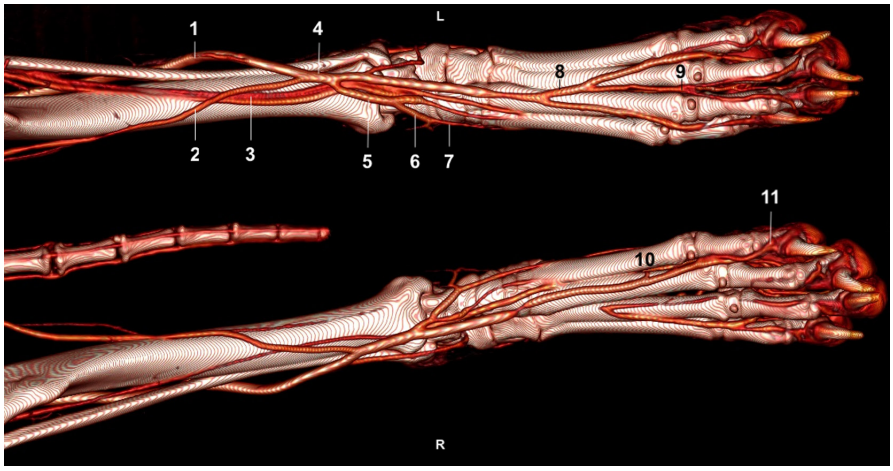

FIGURE 4 3D VRT CT images of the normal lower limb and paw of a dog in the venous phase of angiography from dorsal perspective. The dogs were positioned in sternal recumbency. (R) Right; (L) left. (1) cranial branch of the left lateral saphenous vein; (2) cranial branch of left medial saphenous vein; (3) left dorsal pedal vein and artery; (4) anastomosis and in parts common course of the left cranial branches of the medial and lateral saphenous veins; (5) cranial branch of left medial saphenous vein; (6) left medial tarsal vein; (7) left superficial plantar branch of medial tarsal vein; (8) common dorsal digital vein; (9) bifurcation in axial proper dorsal digital vein III and IV; (10) interdigital branch

vein could be identified in its course as a continuation of the deep femoral vein in 14 dogs (46.7%), where it reached into the adductors and rotators and discharged various branches from which the obturator branch (Figure 2e/1) was seen the most with a visibility in 7 dogs (23.2%). Still inside the abdominal cavity, the caudal superficial epigastric vein (Figure 2e/4) branched from the pudendoepigastrical vein, running in cranial direction along the rectus abdominis muscle, detectable in 8 dogs (26.7%). Before their final branching, the caudal lateral superficial vein (Figure 2e/9), which could be traced in 11 dogs (36.6%), originated from the internal iliac vein at the level of the fourth tail vertebra and ran lateral and superficial in the tail. The caudal gluteal vein (Figure 2e/6) could be identified branching out of the internal iliac vein at the level of the lesser sciatic notch in 12 dogs (40%) and proceeded laterally from there. The internal pudendal vein (Figure 2f/8) originated from the internal iliac vein in the region of the ischiadic spine, visible in 4 dogs (13.3%) and ran caudally where a clear traceability was not possible anymore in any of the dogs. The testicular vein (Figure 2f/5) could be followed next to the spermatic cord on his way to the testicles in 5 of the 14 male dogs (35.7%). The proximal caudal femoral vein (Figure 2g/4) branched from the femoral vein directly before the medial saphenous vein and could be followed to the adductor muscles like the medial caudal femoral vein (Figure 2h/1) in 19 dogs (63.3%). The distal caudal femoral vein (Figure 2i/1) appeared as the last branch of the femoral vein and the thickest branch in diameter and released the lateral saphenous vein (Figure 3a/4) at the level of the hollow of the popliteal fossa, both detectable in all 30 dogs.

The popliteal vein (Figure 2i/2 and j/3), visible in 26 dogs (86.7%), continued the femoral vein after the branching of the distal caudal femoral vein at the level of the hollow of the knee and released the genicular veins (Figure 2j/2) that ran to the stifle joint and were traceable in 9 dogs (30%). The popliteal vein proceeded over the popliteal incision to the cranial side of the limb and formed the origin of the cranial tibial vein (Figure 3b/6, c/5 and e/7), visible in 3 dogs (10%). The cranial tibial vein ran lateral and cranial alongside the tibia and continued its further course as the dorsal pedal vein (Figures 3f/6 and 4/3) at the level of the tarsal arch. The dorsal pedal vein anastomosed with the cranial branch of the medial saphenous vein at the level of the tarsal joint (Figure 3f/6). The cranial and caudal branches of the medial saphenous vein (Figure 3b/4 and 5) arose distal of the stifle joint. While the cranial branch ran on the lower leg to cranial and anastomosed in various ways with the cranial branch of the lateral saphenous vein, the caudal branch ran along the back of the lower leg to the ankle joint, where it divided into the medial and the lateral plantar vein (Figure 3g/3). Both the cranial branch of the medial saphenous vein and the caudal branch were visible in 29 dogs (96.7%). The cranial and caudal branches of the lateral saphenous vein (Figure 3d/3 and 4) as well as the calcaneal branch (Figure 3d/5) separated from the lateral saphenous vein at the level of the calcaneal tendon. Both branches were visible in all 30 dogs. The cranial branch of the lateral saphenous vein crossed the lower leg laterally and reached the tarsal flexion and anastomosed at this level with the cranial branch of the medial saphenous vein in two different variants (Figure 3e/4 and 5). 6 dogs (20%) showed a common course of the cranial branches of the medial and lateral saphenous veins over a longer distance on the left and right limb (Figure 4/4). On the other hand, 14 dogs (46.7%) showed an anastomosis and immediate separation of the cranial branches of both limbs (Figure 6/1) in both limbs. There were also both variations seen, different on the left and the right limb of 8 dogs (26.7%) (Figure 6/1 and 2). In two dogs (6.6%), the cranial branches of the medial and lateral saphenous veins were not visible. One of these dogs showed no anastomosis of the branches, and in the other dog, the veins were not detectable.

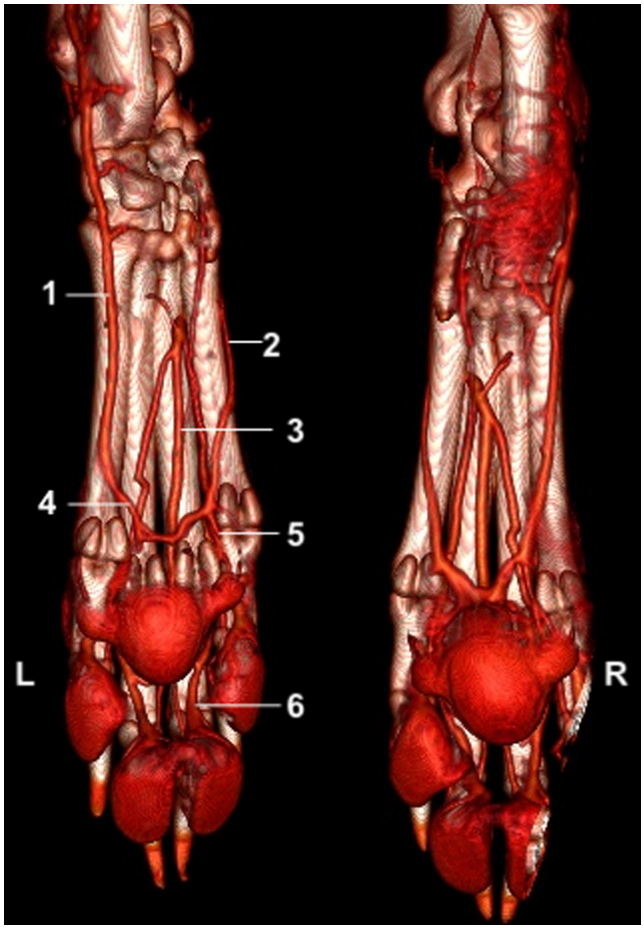

FIGURE 5 3D VRT CT images of the normal lower limb and paw of a dog in the venous phase of angiography in plantar view. The dogs were positioned in sternal recumbency. (R) Right limb; (L) left limb. (1) left superficial branch of caudal branch of lateral saphenous vein; (2) left superficial plantar branch of medial tarsal vein; (3) left plantar metatarsal vein III; (4) left superficial plantar arch; (5) left common plantar digital vein II; (6) left proper plantar digital vein

The cranial branches of the saphenous veins branched off the medial and the lateral tarsal veins (Figure 3e/10, f/5, 8 and g/4) at the level of the tarsal arch, where the medial tarsal vein immediately built the origin of the superficial plantar branch (Figure 3f/4, h/2, 4/7, 5/2). The medial and lateral tarsal veins were visible in 23 dogs (76.7%). The caudal branch of the lateral saphenous vein (Figure 3d/4) followed the lateral side of the tarsus and paw (Figure 3e/5) and united with the superficial plantar branch (Figure 3f/4) from the medial side to form the superficial plantar arch (Figure 5/4), well visible in 17 dogs (56.7%). The dorsal metatarsal veins branching off the deep dorsal arch could not be represented visually. The common and proper dorsal digital veins (Figure 3g and h) were visible superficial under the skin of the paws of 29 dogs (96.7%).

The plantar metatarsal veins, traceable in all 28 dogs (93.3%), emerged from the deep plantar arch (Figure 3f and g) visible in two dogs (6.7%) and ended in the superficial plantar branch, which built

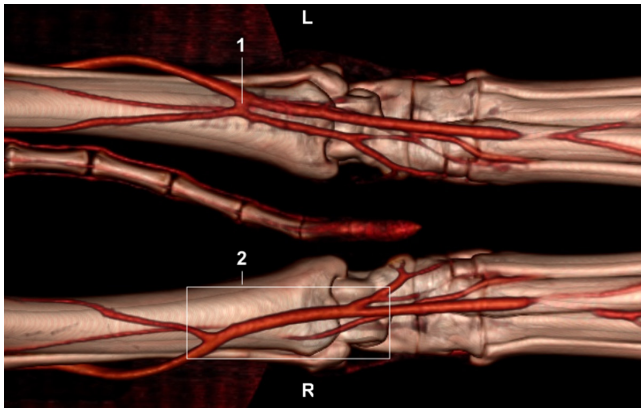

FIGURE 6 3D VRT CT images of the normal lower limb and talocalcaneal joint of a dog in the venous phase of angiography. In this image, the two normal variants of the anastomosis of the cranial branches of the saphenous veins can be recognized, which were traceable in many dogs. (R) Right limb; (L) left limb. (1) anastomosis and immediately separation of the cranial branches of the left medial and lateral saphenous veins; (2) anastomosis and in parts common course of the right cranial branches of the medial and lateral saphenous veins

the origin of the common and proper plantar veins (Figure 3g and h), visible in 28 dogs (93.3%). Interdigital branches enabled a communication between the dorsal and plantar venous system (Figure 4) and were detectable in 25 dogs (83.3%).

4 | DISCUSSION

Knowledge of normal venous anatomy serves as the basis for the characterization of venous abnormalities in canine hindlimbs. This study describes in detail the normal anatomy and venous contrast enhancement of the canine hindlimb vasculature using CT-technology. The method of venous phase, 64-slice helical CT angiography and thin slices of 0.6 mm enabled an excellent visibility of the canine hindlimb venous system. Even small veins could be visualized effectively.

But it must be noted that there are now scanners with more detector rows that could allow even faster scans, which could increase the chances to match the venous phase more reliably. The use of bolus-tracking software enabled automatic detection of a set threshold of contrast agent accumulation in the abdominal aorta, at which point the arterial scan was automatically started. But bolus tracking does not allow reasonable setting of a threshold of contrast agent accumulation in the caudal vena cava. To achieve an ideal venous phase, a test bolus procedure could have been used for the CT scans. However, these dogs received clinical contrast application for various diagnostic purposes and did not present specifically for venography at the Clinic for Small Animal Surgery and Reproduction. Based on the clinical questions, the primary choice was to image the arterial phase. The venous phase was included to the multiphase scan after the arterial phase. In

humans, Muroga et al. (2021) showed in her study that a split-bolus protocol with an optimized timing was able to achieve better image quality than a single-bolus protocol in 3D CT angiography/venography. For this study, existing data of the scanned venous phases were retrospectively analysed. Test-bolus procedure was not used in these dogs due to the limitations of rapid clinical practice and to prevent prolongation of the dogs' general anaesthesia. Test-bolus or split-bolus method CT angiography may need to be used for even better venous visibility in future studies.

The images selected for this study were mainly transverse images. But it was also possible to create maximum intensity projections (MIP) and 3D images using volume rendering technique from the images obtained. MIP are especially useful for small vessels (Prokop et al., 1997). Stair step and volume-averaging artefacts using MIP are less likely compared to other diagnostic methods (Soyer et al., 1996). This also enabled us to obtain detailed images even of the small veins.

In human medicine to assess limb veins, colour and duplex ultrasound is used especially for the diagnosis of deep venous thrombosis (Gaitini, 2007). Other studies postulate that the veins can be detected just as well in computed tomography venography (CTV) as in Doppler sonography, while the proximal and pelvic veins are only assessable in CTV, which is a great advantage over sonography (Cham et al., 2000; Lim et al., 2004). Lee et al. stated that CTV has an adequate image quality for the evaluation of the veins of the lower extremities (Lee et al., 2008), what we were able to reproduce in our study.

Nevertheless, magnet resonance imaging (MRI) shows to be a more detailed imaging option to also display the surrounding soft tissue of peripheral veins (Voigts et al., 2017). When searching for deep venous thrombosis, magnet resonance venography (MRV) can even differentiate acute from chronic thrombosis and diagnose central obstructions in the veins, which represents a clear advantage over CTV (Gaitini, 2007).

As another non-invasive technique for imaging vasculature in dogs, Bruehschwein et al. performed contrast-enhanced magnetic resonance angiography (CE-MRA) (Bruehschwein et al., 2010). This study showed a sufficient imaging of the abdominal and portosystemic vasculature. It also enables MIP images but is comparatively less effective than CTA in terms of cost–benefit ratio. In human medicine, CE-MRA is also used for imaging the lower extremity vasculature (Yi et al., 2016). Further studies must show whether this method could also be useful for imaging canine hindlimb veins.

A general disadvantage of angiography using contrast media is the various possible side effects, such as headache, nausea, vomiting, iodine poisoning, respiratory distress, cardiac arrhythmia, contrast-induced nephropathy, contrast-induced encephalopathy or anaphylactic shock (Chandiramani et al., 2020; De Rycke et al., 2014; Spina et al., 2017). Especially, contrast-induced kidney damage in dogs has been observed (Goic et al., 2016; Scarabelli et al., 2016) but to a much lesser extent than in humans. Recent studies show that carbon dioxide could be an adequate alternative to iodine-containing contrast media (Pedersoli et al., 2019).

Limitations of this study were the relatively small group of only 30 dogs investigated and the variation in the bodyweight of the dogs. Three dogs needed to be positioned in frog position of the hindlimbs, but this did not seem to affect the visibility of the small veins. The different visibilities of the veins in the different size dogs made providing a complete description of the venous vessels of the canine hindlimbs more difficult. Smaller veins seem to make imaging with CTA more difficult. But possible reasons for this inconsistent enrichment and visualization of the veins in different dogs need further investigation in the future, which this group of investigators aims to archive.

In this study, we were able to describe and picture all bigger venous vessels of the canine hindlimb and the most important of their branches. The variation in the course of the cranial branches of the medial and lateral saphenous vein we observed was described in anatomic literature earlier (Waibl and Wilkens, 2005). But in this study, we were successful in visualizing this variation in a 3D image.

In conclusion, this study provided a complete description of the venous vessels of dog's hindlimbs in CT images and gives the practitioner an advantage in diagnosing abnormal changes and planning surgical interventions.

ACKNOWLEDGEMENTS

The authors wish to thank Dr. Maike Schroers for her kind support with both, general and technical matters. Open Access funding enabled and organized by Projekt DEAL.

CONFLICT OF INTEREST

The authors declare that there is no conflict of interest.

DATE AVAILABILITY STATEMENT

The data that support the findings of this study are available from the corresponding author K.T.B. upon reasonable request. Whenever possible, the persistent identifier (DOI) was inserted along the reference.

ORCID

Klara Theresia Besuden https://orcid.org/0000-0002-6194-756X
Andrea Meyer-Lindenberg https://orcid.org/0000-0001-6137-3773
Andreas Brühschwein https://orcid.org/0000-0002-7833-8031

REFERENCES

Aquila, A. M. (2001). Deep venous thrombosis. *The Journal of Cardiovascular Nursing*, *15*(4), 25–44. https://doi.org/10.1097/00005082-200107000-00004

Bruehschwein, A., Foltin, I., Flatz, K., Zoellner, M., & Matis, U. (2010). Contrast-enhanced magnetic resonance angiography for diagnosis of portosystemic shunts in 10 dogs. *Veterinary Radiology & Ultrasound*, *51*(2), 116–121. https://doi.org/10.1111/j.1740-8261.2009.01634.x

Budras, K.-D., Reese, S., Mülling, C., Pfarrer, C., & Kölle, S. (2007). *Atlas der Anatomie des Hundes: Lehrbuch für Tierärzte und Studierende*. Schlütersche.

Cham, M. D., Yankelevitz, D. F., Shaham, D., Shah, A. A., Sherman, L., Lewis, A., & Henschke, C. I. (2000). Deep venous thrombosis: Detection by using indirect CT venography. The pulmonary

angiography-indirect CT venography cooperative group. *Radiology*, *216*(3), 744–751.

Chandiramani, R., Cao, D., Nicolas, J., & Mehran, R. (2020). Contrast-induced acute kidney injury. *Cardiovascular Intervention and Therapeutics*, *35*(3), 209–217.

De Rycke, L. M., Kromhout, K. J., van Bree, H. J., Bosmans, T., & Gielen, I. M. (2014). Computed tomography atlas of the normal cranial canine abdominal vasculature enhanced by dual-phase angiography. *Anatomia, Histologia, Embryologia*, *43*(6), 413–422.

Erdmann, A., Alatri, A., Engelberger, R. P., Depairon, M., Calanca, L., & Mazzolai, L. (2015). Suspicion of lower limb deep vein thrombosis: Update on diagnosis and treatment. *Revue Médicale Suisse*, *11*(460), 337–341.

Gaitini, D. (2007). Multimodality imaging of the peripheral venous system. *International Journal of Biomedical Imaging*, *2007*, 54616. https://doi.org/10.1155/2007/54616

Goic, J. B., Koenigshof, A. M., McGuire, L. D., Klinger, A. C., & Beal, M. W. (2016). A retrospective evaluation of contrast-induced kidney injury in dogs (2006-2012). *Journal of Veterinary Emergency and Critical Care (San Antonio, Tex.)*, *26*(5), 713–719. https://doi.org/10.1111/vec.12511

Habermehl, K. H., Nickel, R., Schummer, A., & Seiferle, E. (2005). *Lehrbuch der Anatomie der Haustiere: Band III Kreislaufsystem, Haut und Hautorgane (Vol. 4. unveränderte Auflage)*. Parey.

Kanne, J. P., & Lalani, T. A. (2004). Role of computed tomography and magnetic resonance imaging for deep venous thrombosis and pulmonary embolism. *Circulation*, *109*(12 Suppl 1), I15–I21. https://doi.org/10.1161/01.Cir.0000122871.86662.72

Katz, D. S., Loud, P. A., Bruce, D., Gittleman, A. M., Mueller, R., Klippenstein, D. L., & Grossman, Z. D. (2002). Combined CT venography and pulmonary angiography: A comprehensive review. *Radiographics*, *22*, S3-19; discussion S20-14. https://doi.org/10.1148/radiographics.22.suppl_1.g02oc17s3

Lee, W., Chung, J. W., Yin, Y. H., Jae, H. J., Kim, S. J., Ha, J., & Park, J. H. (2008). Three-dimensional CT venography of varicose veins of the lower extremity: Image quality and comparison with doppler sonography. *American Journal of Roentgenology*, *191*(4), 1186–1191. https://doi.org/10.2214/ajr.07.3471

Lim, K. E., Hsu, W. C., Hsu, Y. Y., Chu, P. H., & Ng, C. J. (2004). Deep venous thrombosis: Comparison of indirect multidetector CT venography and sonography of lower extremities in 26 patients. *Clinical Imaging*, *28*(6), 439–444. https://doi.org/10.1016/s0899-7071(03)00319-x

Liu, P., Peng, J., Zheng, L., Lu, H., Yu, W., Jiang, X., & Zhao, Z. (2018). Application of computed tomography venography in the diagnosis and severity assessment of iliac vein compression syndrome: A retrospective study. *Medicine (Baltimore)*, *97*(34), e12002. https://doi.org/10.1097/md.0000000000012002

Muroga, K., Ichikawa, K., Maruyama, A., & Ihara, N. (2021). Split-bolus injection protocol with optimized timings of contrast medium injection and CT scanning for 3D CT angio-venography before laparoscopic gastrectomy. *Japanese Journal of Radiology*, *39*(4), 395–403. https://doi.org/10.1007/s11604-020-01069-2

Otto, C. M., Rieser, T. M., Brooks, M. B., & Russell, M. W. (2000). Evidence of hypercoagulability in dogs with parvoviral enteritis. *Journal of the American Veterinary Medical Association*, *217*(10), 1500–1504. https://doi.org/10.2460/javma.2000.217.1500

Pedersoli, F., Bruners, P., Kuhl, C. K., & Schmitz-Rode, T. (2019). Current CO(2) angiography. *Radiologe*, *59*(6), 533–540. https://doi.org/10.1007/s00117-019-0533-6

Prokop, M., Shin, H. O., Schanz, A., & Schaefer-Prokop, C. M. (1997). Use of maximum intensity projections in CT angiography: A basic review. *Radiographics*, *17*(2), 433–451. https://doi.org/10.1148/radiographics.17.2.9084083

Scarabelli, S., Cripps, P., Rioja, E., & Alderson, B. (2016). Adverse reactions following administration of contrast media for diagnostic imaging in anaesthetized dogs and cats: A retrospective study. *Veterinary Anaesthesia and Analgesia*, *43*(5), 502–510. https://doi.org/10.1111/vaa.12335

Shiver, S. A., Lyon, M., Blaivas, M., & Adhikari, S. (2010). Prospective comparison of emergency physician-performed venous ultrasound and CT venography for deep venous thrombosis. *The American Journal of Emergency Medicine*, *28*(3), 354–358. https://doi.org/10.1016/j.ajem.2009.01.009

Soyer, P., Heath, D., Bluemke, D. A., Choti, M. A., Kuhlman, J. E., Reichle, R., & Fishman, E. K. (1996). Three-dimensional helical CT of intrahepatic venous structures: Comparison of three rendering techniques. *Journal of Computer Assisted Tomography*, *20*(1), 122–127. https://doi.org/10.1097/00004728-199601000-00023

Spina, R., Simon, N., Markus, R., Muller, D. W., & Kathir, K. (2017). Contrast-induced encephalopathy following cardiac catheterization. *Catheterization and Cardiovascular Interventions*, *90*(2), 257–268. https://doi.org/10.1002/ccd.26871

Stehling, M. K., Rosen, M. P., Weintraub, J., Kim, D., & Raptopoulos, V. (1994). Spiral CT venography of the lower extremity. *American Journal of Roentgenology*, *163*(2), 451–453. https://doi.org/10.2214/ajr.163.2.8037048

Voigts, B., Abolmaali, N., Stelzner, C., & Schellong, S. M. (2017). Imaging representation of peripheral veins. *Internist*, *58*(8), 796–804. https://doi.org/10.1007/s00108-017-0281-5

Waibl, H., & Wilkens, H. (2005). *Lehrbuch der Anatomie der Haustiere: Kreislaufsystem, Haut und Hautorgane*. Parey.

Wright, M. P., Smeds, M. R., Wright, L., & Ali, A. T. (2017). High-resolution CT angiogram for lower extremity vein mapping. *The American Surgeon*, *83*(3), 257–259. https://doi.org/10.1177/000313481708300320

Yi, C. Y., Zhou, D. X., Li, H. H., Wang, Y., Chen, K., Chen, J., & Xu, X. L. (2016). Comparison of imaging value for diabetic lower extremity arterial disease between FBI and CE-MRA. *European Review for Medical and Pharmacological Sciences*, *20*(14), 3078–3086.

Zerhouni, E. A., Barth, K. H., & Siegelman, S. S. (1980). Demonstration of venous thrombosis by computed tomography. *American Journal of Roentgenology*, *134*(4), 753–758. https://doi.org/10.2214/ajr.134.4.753

How to cite this article: Besuden, K. T., Meyer-Lindenberg, A. & Brühschwein, A. (2022). Computed tomography venography description of the normal anatomy of the canine hindlimb venous system. *Anatomia, Histologia, Embryologia*, *51*, 459–467. https://doi.org/10.1111/ahe.12806